estimated between 20,000 and 40,000 metric tons (*10*, *12*). Assuming that pre-Incan technologies operated at efficiencies comparable to *huayras* and recognizing the initial presence of grades as rich as 25% Ag (*11*), our data imply that several thousand tons of silver were produced in pre-Incan times. Although major new archaeological discoveries in the Andes remain a distinct possibility, the likelihood seems equally probable that most of this silver was recycled and transported elsewhere in the Americas before conquest, or eventually exported overseas by the Spanish.

References and Notes

1. H. Lechtman, in *The Coming of the Age of Iron*, P. J. Wertime, J. D. Muhly, Eds. (Yale Univ., New Haven, CT, 1980), pp. 267–334.
2. R. L. Burger, R. B. Gordon, *Science* **282**, 1108 (1998).
3. E. P. Benson, Ed., *Pre-Columbian Metallurgy of South America* (Dumbarton Oaks, Washington, DC, 1979).
4. I. Shimada, S. Epstein, A. K. Craig, *Science* **216**, 952 (1982).
5. H. Lechtman, in *Tiwanaku and Its Hinterland: Archaeology and Paleoecology of an Andean Civilization Vol. 2*, A. L. Kolata, Ed. (Smithsonian Institution, Washington, DC, 2002), pp. 404–434.
6. K. O. Bruhns, *Ancient South America* (Cambridge Univ., Cambridge, 1994).
7. W. E. Rudolph, *Am. Geogr. Soc.* **26**, 529 (1936).
8. M. Vuille, *Int. J. Climatol.* **19**, 1579 (1999).
9. Materials and methods are available as supporting material on *Science* Online.
10. P. J. Bartos, *Econ. Geol.* **95**, 645 (2000).
11. W. E. Wilson, A. Petrov, *Miner. Rec.* **30**, 9 (1999).
12. P. J. Bakewell, *Miners of the Red Mountain: Indian Labor in Potosí 1545-1650* (Univ. of New Mexico, Albuquerque, NM, 1984).
13. R. Peele, *Sch. Mines Q.* **15**, 8 (1893).
14. I. Renberg, I. M. Wik-Persson, O. Emteryd, *Nature* **368**, 323 (1994).
15. M. L. Brännvall, R. Bindler, O. Emteryd, I. Renberg, *J. Paleolimnol.* **25**, 421 (2001).
16. C. Gobeil, *Environ. Sci. Technol.* **33**, 2953 (1999).
17. I. Rivera-Duarte, A. R. Flegal, *Geochim. Cosmochim. Acta* **58**, 3307 (1994).
18. B. B. Wolfe, *Palaeogeogr. Palaeoclim. Palaeoecol.* **176**, 177 (2001).
19. A. S. Ek, I. Renberg, *J. Paleolimnol.* **26**, 89 (2001).
20. A. F. Bandelier, *The Islands of Titicaca and Koati* (Hispanic Society of America, New York, 1910).
21. P. R. Williams, *World Archaeol.* **33**, 361 (2002).
22. A. L. Kolata, *The Tiwanaku: Portrait of an Andean Civilization* (Blackwell, Oxford, UK, 1993).
23. M. B. Abbott, M. W. Binford, M. Brenner, K. R. Kelts, *Quat. Res.* **47**, 169 (1997).
24. B. S. Bauer, C. Stanish, *Ritual and Pilgrimage in the Ancient Andes: The Islands of the Sun and the Moon* (Univ. of Texas, Austin, TX, 2001).
25. L. G. Thompson, E. Mosley-Thompson, J. F. Bolzan, B. R. Koci, *Science* **229**, 971 (1985).
26. A. K. Craig, in *Precious Metals, Coinage, and the Changes in Monetary Structures in Latin America, Europe, and Asia*, E. van Cauwenberghe, Ed. (Leuven Univ. Press, Leuven, Netherlands, 1989), pp. 159–183.
27. G. E. Ericksen, R. G. Luedke, R. L. Smith, R. P. Koeppen, F. Urquidi, *Episodes* **13**, 5 (1990).

28. Supported by the U.S. NSF-ESH (M.B.A), Natural Sciences and Engineering Research Council of Canada (A.P.W.) and Geological Society of America. We are grateful to H. Lechtman, M. Bermann, C. Cooke; and journal reviewers for their insightful comments; G. Seltzer for assistance in the field; and S. Root for support in the laboratory.

Supporting Online Material

www.sciencemag.org/cgi/content/full/301/5641/1893/DC1
Materials and Methods
Fig. S1
Tables S1 and S2

9 June 2003; accepted 18 August 2003

Inactivation of TNF Signaling by Rationally Designed Dominant-Negative TNF Variants

Paul M. Steed,* Malú G. Tansey,*† Jonathan Zalevsky,* Eugene A. Zhukovsky, John R. Desjarlais, David E. Szymkowski, Christina Abbott, David Carmichael, Cheryl Chan, Lisa Cherry, Peter Cheung, Arthur J. Chirino, Hyo H. Chung, Stephen K. Doberstein, Araz Eivazi, Anton V. Filikov, Sarah X. Gao, René S. Hubert, Marian Hwang, Linus Hyun, Sandhya Kashi, Alice Kim, Esther Kim, James Kung, Sabrina P. Martinez,† Umesh S. Muchhal, Duc-Hanh T. Nguyen, Christopher O'Brien, Donald O'Keefe, Karen Singer, Omid Vafa, Jost Vielmetter, Sean C. Yoder, Bassil I. Dahiyat‡

Tumor necrosis factor (TNF) is a key regulator of inflammatory responses and has been implicated in many pathological conditions. We used structure-based design to engineer variant TNF proteins that rapidly form heterotrimers with native TNF to give complexes that neither bind to nor stimulate signaling through TNF receptors. Thus, TNF is inactivated by sequestration. Dominant-negative TNFs represent a possible approach to anti-inflammatory biotherapeutics, and experiments in animal models show that the strategy can attenuate TNF-mediated pathology. Similar rational design could be used to engineer inhibitors of additional TNF superfamily cytokines as well as other multimeric ligands.

TNF is a proinflammatory cytokine that can complex two TNF receptors, TNFR1 (p55) and TNFR2 (p75), to activate signaling cascades controlling apoptosis, inflammation, cell proliferation, and the immune response (*1*–*5*). The 26-kD type II transmembrane TNF precursor protein, expressed on many cell types, is proteolytically converted into a soluble 52-kD homotrimer (*6*). An elevated serum level of TNF is associated with the pathophysiology of rheumatoid arthritis (RA), inflammatory bowel disease, and ankylosing spondylitis (*1*, *7*, *8*), and molecules that inhibit TNF signaling have demonstrated clinical efficacy in treating some of these diseases (*9*, *10*).

We have engineered dominant-negative TNF (DN-TNF) variants that inactivate the native homotrimer by a sequestration mechanism that blocks TNF bioactivity (fig. S1). Protein design automation (PDA), an in silico method that predicts protein variants with improved biological properties (*11*–*13*), was used to introduce single or double amino acid changes into TNF (Fig. 1A) to generate the desired biological profile while maintaining the overall structural integrity of the molecule. Specifically, our goal was to design homotrimeric TNF variants that (i) have decreased receptor binding, (ii) sequester native TNF homotrimers from TNF receptors by formation of inactive native:variant heterotrimers, (iii) abolish TNF signaling in relevant biological assays, and (iv) are easily expressed and purified in large quantities from bacteria. Variants were tested for TNF receptor activation in cell-based assays, and nonagonistic variants were then checked for their ability to antagonize native TNF in cell and animal models. Subsequently, we evaluated assembly state, receptor binding, and heterotrimer formation for several variants.

The computational design strategy used crystal structures of native and variant TNF trimers as templates for the simulations. Analysis of a homology model of the TNF-receptor complex revealed several distinct regions of the cytokine that make multiple direct contacts with its receptors (Fig. 1A), including interfaces rich in hydrophobic and electrostatic interactions. We ran simulations to select nonimmunogenic point mutations that would disrupt receptor interactions while preserving the structural integrity of the TNF variants and their ability to assemble into heterotrimers with native TNF (*14*). Many of the designed TNF variants displayed markedly reduced binding to TNFR1 and TNFR2, and several combinations of potent single mutations further decreased binding (Fig. 1B and fig. S2). As predicted by analysis of the TNF-TNFR structural complex, combinations of the most potent single mutations at different interaction domains (e.g., A145R and

Xencor, 111 West Lemon Avenue, Monrovia, CA 91016, USA.

*These authors contributed equally to this work.
†Present address: Department of Physiology, University of Texas Southwestern Medical Center at Dallas, Dallas, TX 75390, USA.
‡To whom correspondence should be addressed. E-mail: baz@xencor.com

I97T) were frequently additive or synergistic. Moreover, our data extend results of previous studies (*15*, *16*) in demonstrating that certain substitutions can alter the specificity of receptor interactions; for example, I97T and A145R/I97T show greater relative binding to TNFR2 than to TNFR1 (Fig. 1B and fig. S2).

Homotrimers of several designed TNF variants exhibited >10,000-fold reduction in their ability to activate two major signaling pathways downstream of TNF receptor activation. Specifically, single variants such as Y87H and A145R and the double variant A145R/Y87H were unable to bind to either TNFR1 or TNFR2 in cell-free assays (Fig. 1B and fig. S2) and failed to activate either caspase (Fig. 1C) or nuclear factor κB (NF-κB)–mediated luciferase expression (Fig. 1D) relative to native TNF. In contrast, those variants that still bound TNFRs also activated TNF signaling, in some cases (e.g., F144N) more potently than native TNF. Disruption of two receptor interfaces (e.g., A145R/Y87H or A145R/I97T) effectively destroyed the residual agonism detected with some single-point TNF variants. Furthermore, the importance of using multiple screening criteria to evaluate DN-TNF bioactivity was revealed by variants such as A145R/I97T, which had virtually no TNF-like activity in either cell-based assay yet displayed appreciable TNFR2 binding affinity.

We subsequently tested nonagonistic TNF variants for their ability to act as dominant-negative inhibitors by measuring their capacity to block native TNF activity in cell-based assays. We evaluated dose-dependent TNF antagonism (*14*) by mixing increasing concentrations of variants with native TNF (5 ng/ml) for 1.5 hours and measuring the caspase activity induced by these mixtures after addition to U937 cells (Fig. 2A). At concentrations as low as twofold that of native TNF (10 ng/ml), A145R/Y87H and

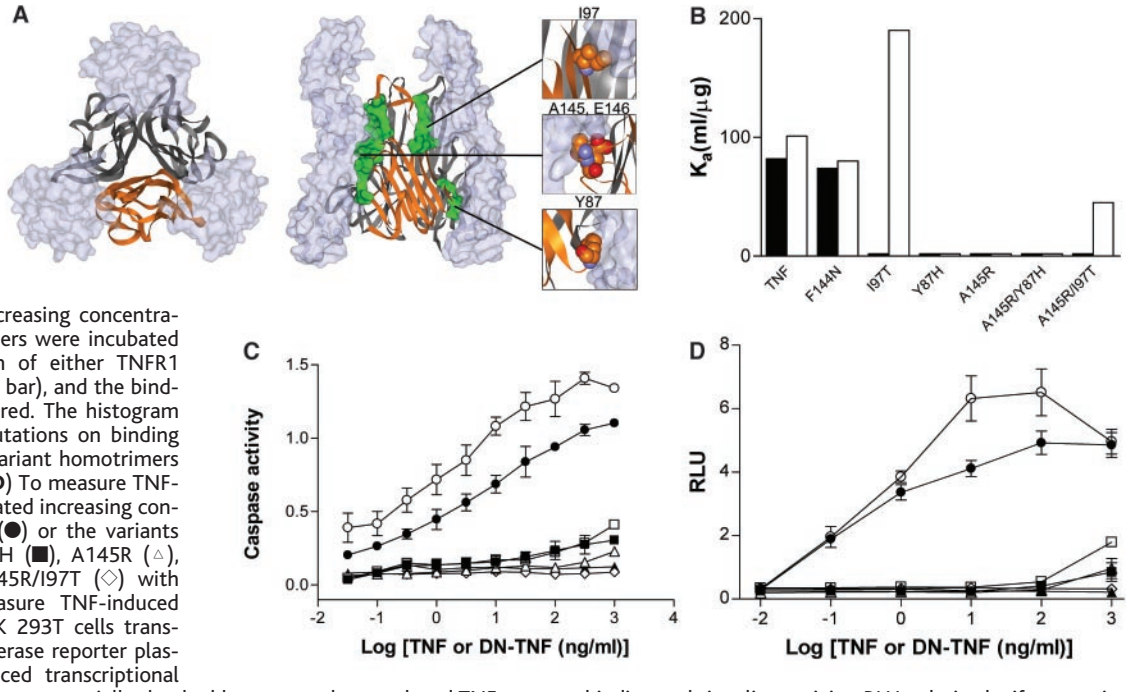

Fig. 1. DN-TNF variants have impaired TNF receptor binding and signaling. (**A**) Structural schematic of human TNF trimer–TNFR1 complex with major contacts between ligand and receptor highlighted by solid surfaces (green). Locations of representative mutated residues substituted in dominant-negative variants are shown in boxes. (**B**) Increasing concentrations of DN-TNF homotrimers were incubated with a fixed concentration of either TNFR1 (black bar) or TNFR2 (white bar), and the binding affinity (K_a) was measured. The histogram illustrates the effect of mutations on binding affinity between DN-TNF variant homotrimers and TNF receptors. (**C** and **D**) To measure TNF-induced signaling, we incubated increasing concentrations of native TNF (●) or the variants F144N (○), I97T (□), Y87H (■), A145R (△), A145R/Y87H (▲), and A145R/I97T (◇) with either U937 cells to measure TNF-induced caspase activity (C) or HEK 293T cells transfected with an NF-κB–luciferase reporter plasmid to measure TNF-induced transcriptional activation (D). DN-TNF variants, especially the double mutants, have reduced TNF receptor binding and signaling activity. RLU, relative luciferase units; Caspase activity, arbitrary units normalized to V_{max}.

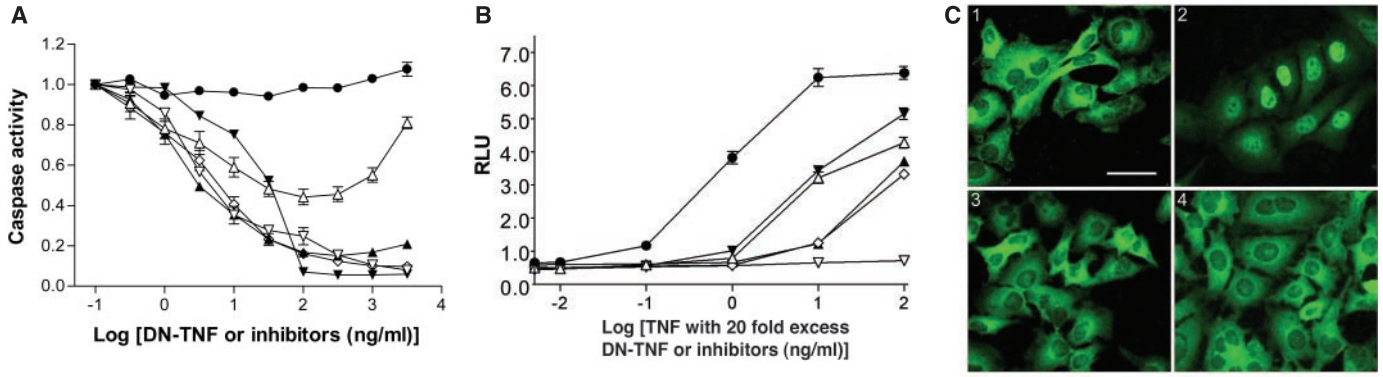

Fig. 2. DN-TNF variants inhibit TNF-mediated intracellular signaling. (**A**) Inhibition of caspase activation. Native TNF (5 ng/ml) was mixed with buffer (●) or with increasing concentrations of either TNF variants A145R (△), A145R/Y87H (▲), or A145R/I97T (◇), the soluble Fc-TNFR2 fusion etanercept (▽), or the TNF monoclonal antibody infliximab (▼). After 1.5 hours of incubation in exchange buffer (*14*), these mixtures were applied to U937 cells to stimulate caspase activity. (**B**) Inhibition of NFκB pathway activation. Native TNF (●) (25 μg/ml) was mixed with 20-fold excess (by mass) of A145R (△), A145R/Y87H (▲), A145R/I97T (◇), etanercept (▽), or infliximab (▼). These mixtures were serially diluted and applied to HEK 293T cells for 12 hours to induce NF-κB–luciferase reporter activity. (**C**) A145R/Y87H inhibits native TNF-induced nuclear translocation of the p65-RelA subunit of NF-κB. Immunofluorescence studies show subcellular localization of NF-κB in HeLa cells treated with buffer (panel 1), native TNF (10 ng/ml) (panel 2), A145R/Y87H (100 ng/ml) (panel 3), or the combination of native TNF and variant A145R/Y87H (panel 4). RLU, relative luciferase units; Caspase activity, arbitrary units normalized to V_{max}. Scale bar, 25 μm.

A145R/I97T attenuated TNF-induced caspase activity by 50%, and at 20-fold excess, activity was reduced to baseline. The in vitro potency (by mass) of these variants is comparable to that of a soluble Fc-TNFR2 fusion (etanercept) and more potent than that of an antibody to TNF (infliximab), two marketed anti-TNF therapies, supporting the potential utility of this mechanism. Similarly, at 20-fold excess over native TNF, single-point (A145R, I97T, Y87H) and particularly double-point (A145R/Y87H, A145R/I97T) variants decreased caspase activation (fig. S3) as well as TNF-induced transcriptional activation by NF-κB in human embryonic kidney (HEK) 293T cells (Fig. 2B). Consistent with these results, the TNF variant A145R/Y87H (at 10-fold excess over native TNF) blocked TNF-induced nuclear translocation of the NF-κB p65-RelA subunit in HeLa cells (Fig. 2C). Thus, a number of variants neutralized TNF-induced caspase and NF-κB–mediated transcriptional activity over a wide range of native TNF concentrations, including the clinically relevant range of 100 to 200 pg/ml found in the synovial fluid of RA patients (*17*–*19*).

To demonstrate that the mechanism of TNF inhibition requires the formation of heterotrimeric complexes with native TNF, we measured the relation between heterotrimer levels and inhibition of TNF-induced signaling (*14*). We generated heterotrimeric complexes by mixing a fixed amount of FLAG-tagged native TNF with increasing concentrations of His-tagged TNF variants. A part of this material was used in a sandwich enzyme-linked immunosorbent assay (ELISA) (Fig. 3A, open symbols) to detect the formation of His-FLAG heterotrimers, and the remainder was applied to U937 cells to detect TNF-mediated caspase activation (Fig. 3A, closed symbols). The extent of heterotrimer formation of A145R/Y87H or A145R/I97T with native TNF correlated with a decrease in caspase activation, demonstrating an inverse relation between signaling and heterotrimer formation. As expected, etanercept activity is independent of TNF monomer exchange (Fig. 3A, open circles) because etanercept binds to the TNF trimer. To directly visualize heterotrimer formation, we mixed FLAG-tagged native TNF with His-tagged DN-TNF and resolved the exchanged products using native polyacrylamide gel electrophoresis (PAGE) (Fig. 3B) (*20*). Electrophoresis of equimolar quantities of mixed DN-TNF and native TNF resolved the variant homotrimer, 1:2 and 2:1 native:variant heterotrimers, and native homotrimer in approximately the expected 1:3:3:1 ratio (Fig. 3B, lane 10:10). Western blot analyses (*14*) with antibodies against the epitope tags confirmed the composition of the intermediate species (fig. S4). Stochastic equilibrium modeling of native and variant TNF heterotrimer assembly predicts that 10-fold excess of variant homotrimer causes the loss of more than 99% of homotrimeric native TNF, primarily into 1:2 native:variant heterotrimers, and our results confirmed this (Fig. 3B, lane 10:100). Exchange reactions between native and variant TNF reached ~80% completion at 20 min, and essentially all the native homotrimer was depleted after 90 min (fig. S5). Finally, we confirmed that biological activity of variants requires exchange into heterotrimeric complexes with native TNF. Specifically, our most potent variants (e.g., A145R/Y87H) failed to block caspase activity induced by chemically cross-linked native TNF homotrimers (*14*), which are unable to dissociate to allow exchange with variant TNFs (fig. S6).

The most potent in vitro inhibitors were selected for testing in vivo, to further study the mechanism and to begin therapeutic lead candidate identification. We tested the bioactivity of variant homotrimer and native:variant heterotrimers in the D-galactosamine (GalN)-sensitized mouse model, which demonstrated that DN-TNF homotrimers, and heterotrimers with native TNF, are devoid of agonist activity and efficiently exchange with endogenous TNF in vivo. GalN is a known specific hepato-toxin that can increase the sensitivity of mice to human TNF by 1000-fold (*21*, *22*). Native human TNF (30 μg/kg) induced severe hepatocellular apoptosis and lethality, consistent with previous reports

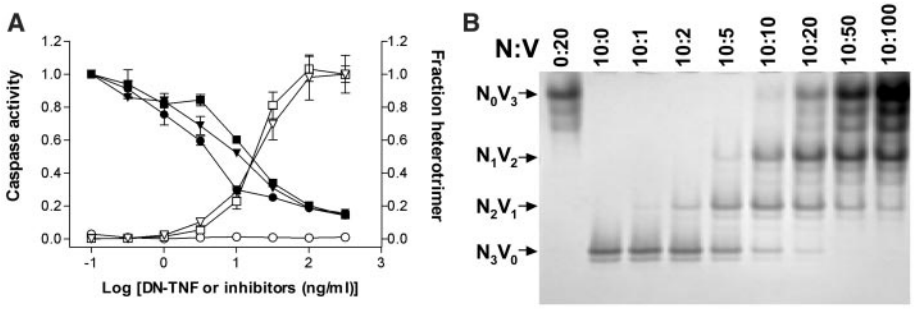

Fig. 3. DN-TNF variants inhibit signaling by sequestering native TNF into inactive heterotrimers. (**A**) Inverse correlation between heterotrimer formation and caspase activity. Native TNF was mixed in exchange buffer (*14*) with A145R/Y87H (▽, ▼), A145R/I97T (□, ■), or etanercept (○, ●), as described for Fig. 2. A part of each mixture was analyzed by a sandwich ELISA to detect native:variant TNF (open symbols), and the remainder was used to stimulate caspase activity in U937 cells (closed symbols). Caspase activity, arbitrary units normalized to V_{max}. (**B**) Native gel analysis of heterotrimer formation with various ratios of native (N) and DN-TNF (V). FLAG-tagged native TNF was incubated alone (N_3:V_0, lane 10:0) or with increasing concentrations of His-tagged variant A145R/Y87H (lanes 10:1 to 10:100) before native gel electrophoresis to determine heterotrimer formation. The differences in isoelectic point conferred by the epitope tags allowed for resolution of all possible trimer species (N_3:V_0, N_2:V_1, N_1:V_2, and N_0:V_3). Increasing concentrations of DN-TNF variant caused the redistribution of native TNF into both heterotrimers, and at 10-fold excess all detectable native TNF was consumed.

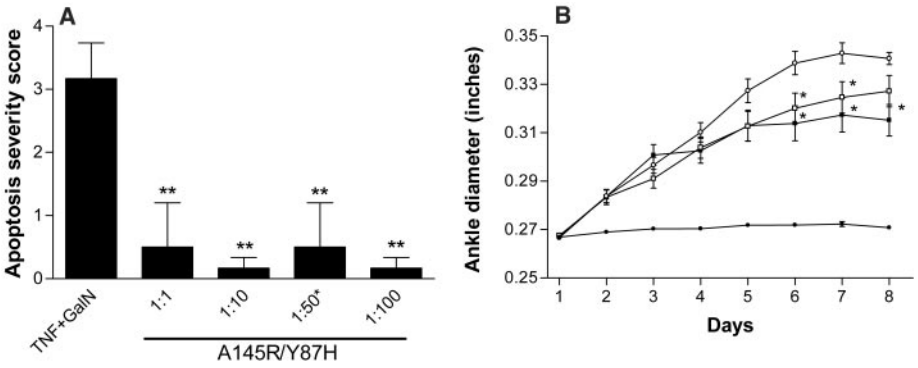

Fig. 4. DN-TNF variants exhibit efficacy in vivo. (**A**) Effect of heterotrimers of various ratios in the galactosamine-sensitized mouse model of human TNF-induced endotoxemia. Native human TNF was dosed at 30 μg/kg and A145R/Y87H was dosed at the indicated ratios to a fixed native human TNF dose of 30 μg/kg except at the 1:50* ratio, where A145R/Y87H was dosed in 50-fold excess of native human TNF (75 μg/kg). Livers were harvested and samples were blinded and scored for apoptotic damage on a scale of 0 to 4 as described (*14*). $^{**}P < 0.05$. (**B**) Efficacy of A145R/Y87H in the rat 7-day established CIA model. A145R/Y87H was modified to introduce a PEG moiety at residue 31 of a non–epitope-tagged molecule as described (*14*). One group of four animals was nonarthritic (●); the remaining animals were collagen treated and, after the onset of symptoms, they were randomized into groups of eight. Animals were treated with vehicle (○), variant at 10 mg/kg twice daily dosing (□), or variant at 2 mg/kg subcutaneously with an intravenous loading dose of 2 mg/kg on the first treatment day (■). Measurements of ankle diameter were made daily by caliper. $^{*}P < 0.05$.

(*23*); in contrast, A145R/Y87H dosed as high as 30 mg per kilogram of mouse body weight (along with native TNF at 30 μg/kg) resulted in no mortality or hepatotoxicity (Fig. 4A) (*24*). Similarly, lethal doses of native human TNF (30 μg/kg) mixed before injection with varying ratios of A145R/Y87H produced no TNF-induced damage. This protection was observed at native: variant ratios as low as 1:1 and with a superlethal dose of TNF (Fig. 4A). Further, sandwich ELISA analyses of serum samples indicated that a substantial portion (30 ng/ml) of administered A145R (3 mg/kg) was in heterotrimers with the endogenous mouse TNF at 1 hour.

A145R/Y87H was next assessed in a model of chronic disease as an initial test of the DN-TNF antagonism mechanism in a disease-relevant setting. We selected the rat 7-day established collagen-induced arthritis (CIA) model because it simulates chronic autoimmune joint disease and can be treated by TNF blockade (*25*). When dosed after the onset of symptoms, only interventions with rapid onset of action would be able to affect disease progression in this model, thus requiring rapid exchange in vivo of TNF variants with endogenous TNF. To ensure that there were no confounding in vivo effects of using affinity-tagged variants, we produced A145R/Y87H that lacked such tags. Further, to decrease in vivo clearance, we added one polyethylene glycol (PEG; ~5 kD/molecule) to each monomeric subunit of A145R/Y87H. This modification had no effect on the dominant-negative properties of the molecule in vitro (fig. S7). A145R/Y87H reduced joint swelling in the CIA model when dosed once daily at 2.0 mg/kg subcutaneously with a loading dose of 2.0 mg/kg and twice daily at 10 mg/kg intravenously (Fig. 4B). These results demonstrate the potential of DN-TNFs to inhibit TNF-mediated inflammation and verify that exchange occurs rapidly enough to affect progression of acute symptoms when dosed therapeutically.

Given their high-yield bacterial production, theoretical low immunogenicity, and unique mechanism of action, DN-TNFs show potential as a new class of anti-inflammatory therapy, particularly because existing methodologies (i.e., PEG modification) can be used to further enhance their pharmacokinetic properties (*26*, *27*). Further, we propose that this dominant-negative approach should be tested for its potential to create inhibitors of other multimeric extracellular signaling molecules, in particular other members of the TNF superfamily (e.g., RANKL, CD40L, and BAFF) that have been implicated in human pathophysiology (*28*, *29*).

References and Notes

1. B. B. Aggarwal, A. Samanta, M. Feldmann, in *Cytokine Reference*, J. J. Oppenheim, M. Feldmann, Eds. (Academic Press, London, 2000).
2. G. Chen, D. V. Goeddel, *Science* **296**, 1634 (2002).
3. D. J. MacEwan, *Cell Signal.* **14**, 477 (2002).
4. M. P. Boldin, T. M. Goncharov, Y. V. Goltsev, D. Wallach, *Cell* **85**, 803 (1996).
5. G. M. Cohen, *Biochem. J.* **326**, 1 (1997).
6. S. R. Ruuls *et al.*, *Immunity* **15**, 533 (2001).
7. M. Feldmann, R. N. Maini, *Annu. Rev. Immunol.* **19**, 163 (2001).
8. B. Beutler, *Immunity* **15**, 5 (2001).
9. M. Feldmann, *Nature Rev. Immunol.* **2**, 364 (2002).
10. R. Goldbach-Mansky, P. E. Lipsky, *Annu. Rev. Med.* **54**, 197 (2003).
11. R. J. Hayes *et al.*, *Proc. Natl. Acad. Sci. U.S.A.* **99**, 15926 (2002).
12. A. V. Filikov *et al.*, *Protein Sci.* **11**, 1452 (2002).
13. P. Luo *et al.*, *Protein Sci.* **11**, 1218 (2002).
14. Materials and methods are available as supporting material on *Science* Online.
15. J. Yamagishi *et al.*, *Protein Eng.* **3**, 713 (1990).
16. X. M. Zhang, I. Weber, M. J. Chen, *J. Biol. Chem.* **267**, 24069 (1992).
17. G. Steiner *et al.*, *Rheumatology* **38**, 202 (1999).
18. T. Horiuchi *et al.*, *Endocr. J.* **46**, 643 (1999).
19. A. K. Ulfgren *et al.*, *Arthritis Rheum.* **43**, 2391 (2000).
20. P. Ameloot, W. Declercq, W. Fiers, P. Vandenabeele, P. Brouckaert, *J. Biol. Chem.* **276**, 27098 (2001).
21. I. Hishinuma *et al.*, *Hepatology* **12**, 1187 (1990).
22. S. Sakaguchi, S. Furusawa, K. Yokota, M. Takayanagi, Y. Takayanagi, *Int. J. Immunopharmacol.* **22**, 935 (2000).
23. P. Brouckaert, C. Libert, B. Everaerdt, W. Fiers, *Lymphokine Cytokine Res.* **11**, 193 (1992).
24. P. M. Steed *et al.*, data not shown.
25. A. M. Bendele *et al.*, *Arthritis Rheum.* **43**, 2648 (2000).
26. K. Sreekrishna *et al.*, *Biochemistry* **28**, 4117 (1989).
27. Y. P. Li *et al.*, *Biol. Pharm. Bull.* **24**, 666 (2001).
28. C. F. Ware, *J. Exp. Med.* **192**, F35-8 (2000).
29. R. M. Locksley, N. Killeen, M. J. Lenardo, *Cell* **104**, 487 (2001).

30. We thank M. Ary for technical assistance with the manuscript.

Supporting Online Material

www.sciencemag.org/cgi/content/full/301/5641/1895/DC1
Materials and Methods
References
Figs. S1 to S7

9 December 2002; accepted 14 August 2003

The Dog Genome: Survey Sequencing and Comparative Analysis

Ewen F. Kirkness,[1] Vineet Bafna,[2]* Aaron L. Halpern,[2]* Samuel Levy,[2]* Karin Remington,[2]* Douglas B. Rusch,[2]* Arthur L. Delcher,[1] Mihai Pop,[1] Wei Wang,[1] Claire M. Fraser,[1] J. Craig Venter[2]

A survey of the dog genome sequence (6.22 million sequence reads; 1.5× coverage) demonstrates the power of sample sequencing for comparative analysis of mammalian genomes and the generation of species-specific resources. More than 650 million base pairs (>25%) of dog sequence align uniquely to the human genome, including fragments of putative orthologs for 18,473 of 24,567 annotated human genes. Mutation rates, conserved synteny, repeat content, and phylogeny can be compared among human, mouse, and dog. A variety of polymorphic elements are identified that will be valuable for mapping the genetic basis of diseases and traits in the dog.

Our understanding of how the human genome functions in health and disease will benefit from comparison of its structure with the genomes of other species (*1*, *2*). The domestic dog is a particularly good example, where an unusual population structure offers unique opportunities for understanding the genetic basis of morphology, behaviors, and disease susceptibility (*3*, *4*). The physical and behavioral characteristics of ~300 dog "breeds" are maintained by restricting gene flow between breeds. Many modern breeds are derived from few founders and have been inbred for desired characteristics. This has led to a species with enormous phenotypic diversity, but with significant homogenization of the gene pool within breeds. Many of the ~360 known genetic disorders in dogs resemble human conditions, and their causes may be more tractable in large dog pedigrees than in small, outbred human families (*4*, *5*). The combination of genetic homogeneity and phenotypic diversity also provides an opportunity to understand the genetic basis of many complex developmental processes in mammals (*6*).

Because of the costs of sequencing mammalian genomes to completion, these projects have been restricted to a few species that are considered to be of greatest value to biomedical research. The decision as to whether future projects should aim for complete sequence coverage of a few more genomes, or whether the existing "reference genomes" can be exploited to characterize a wider variety of genomes that are sequenced to a lower level of coverage, must be made. Here,

[1]The Institute for Genomic Research, Rockville, MD 20850, USA. [2]The Center for Advancement of Genomics, Rockville, MD 20850, USA.

*These authors contributed equally to this work.